Published in final edited form as:
Clin Cancer Res. 2010 October 15; 16(20): 4946–4957. doi:10.1158/1078-0432.CCR-10-1439.

Pharmacokinetic/pharmacodynamic modeling identifies SN30000 and SN29751 as tirapazamine analogs with improved tissue penetration and hypoxic cell killing in tumors

Kevin O. Hicks[1], **Bronwyn G. Siim**[1,3], **Jagdish K. Jaiswal**[1], **Frederik B. Pruijn**[1], **Annie M. Fraser**[1,4], **Rita Patel**[1], **Alison Hogg**[1], **H.D. Sarath Liyanage**[1], **Mary Jo Dorie**[2], **J. Martin Brown**[2], **William. A. Denny**[1], **Michael P. Hay**[1], and **William R. Wilson**[1]

[1]Auckland Cancer Society Research Centre, School of Medical Sciences, The University of Auckland, Private Bag 92019, Auckland, New Zealand [2]Department of Radiation Oncology, Division of Radiation and Cancer Biology, Stanford University, Stanford, California, USA

Abstract

Purpose—Tirapazamine (TPZ) has attractive features for targeting hypoxic cells in tumors but limited clinical activity, in part because of poor extravascular penetration. Here we identify improved TPZ analogs by using a spatially resolved pharmacokinetic/pharmacodynamic (SR-PKPD) model that considers tissue penetration explicitly during lead optimization.

Experimental design—The SR-PKPD model was used to guide progression of 281 TPZ analogs through a hierarchical screen. For compounds exceeding hypoxic selectivity thresholds in single cell cultures, SR-PKPD model parameters (kinetics of bioreductive metabolism, clonogenic cell killing potency, diffusion coefficients in multicellular layers, plasma pharmacokinetics at well tolerated doses in mice) were measured to prioritize testing in xenograft models in combination with radiation.

Results—SR-PKPD-guided lead optimization identified SN29751 and SN30000 as the most promising hypoxic cytotoxins from two different structural subseries. Both were reduced to the corresponding 1-oxide selectively under hypoxia by HT29 cells, with an oxygen dependence quantitatively similar to that of TPZ. SN30000, in particular, showed higher hypoxic potency and selectivity than TPZ in tumor cell cultures and faster diffusion through HT29 and SiHa multicellular layers. Both compounds also provided superior plasma PK in mice and rats at equivalent toxicity. In agreement with SR-PKPD predictions, both were more active than TPZ with single dose or fractionated radiation against multiple human tumor xenografts.

Conclusions—SN30000 and SN29751 are improved TPZ analogs with potential for targeting tumor hypoxia in humans, and illustrate the utility of novel SR-PKPD modeling approaches for lead optimization during anticancer drug development.

Requests for Reprints: William R. Wilson, Auckland Cancer Society Research Centre, The University of Auckland, Private Bag 92019, Auckland, New Zealand. Phone: 64-9-9236883. wr.wilson@auckland.ac.nz.
[3]Current address: Gray Institute for Radiation Oncology & Biology, University of Oxford, Oxford OX4 4GA, United Kingdom
[4]Current address: Wolters Kluwer Pharma Solutions, Auckland, New Zealand.

Conflict of interest: W.R.Wilson, J.M.Brown and W.A. Denny have received remuneration as consultants to Proacta Inc within the last 3 years. M.P. Hay, K.O. Hicks, F.B. Pruijn, B.G. Siim, W.A. Denny and W.R. Wilson are inventors on patents related to SN30000 and SN29751.

Keywords

Hypoxia; benzotriazine *N*-oxides; tirapazamine; SN29751; SN30000; extravascular transport; PKPD models

Introduction

Hypoxia, frequently considered a hallmark of cancer, is a consequence of the inefficient vascularisation of tumors (1). In a number of tumor types hypoxia contributes to progression and is associated with poor prognosis and resistance to therapeutic agents through multiple mechanisms. For example in the context of radiation therapy, hypoxic cells are less sensitive to radiation-induced DNA breakage and cell killing (2), and have increased invasive and metastatic potential (3) leading to failure because of metastatic disease outside the radiation field (4, 5). Additional hypoxia induced through the anti-angiogenic action of radiation (6) enhances tumor regrowth by stimulating vasculogenesis (7). These features, along with the relative absence of hypoxia in normal tissues (8), provide a strong rationale for targeting hypoxia, either by inhibiting pathways required for hypoxic cell survival (9, 10) or through the metabolic activation of bioreductive prodrugs under hypoxic conditions (11–13).

The most thoroughly investigated bioreductive prodrug, tirapazamine (TPZ), showed encouraging indications of activity in early clinical studies (14, 15) but failed to improve overall survival in a recent phase III trial with cisplatin/radiotherapy for advanced head and neck cancer (16). This disappointing outcome was shown to be at least partially due to failure of radiation therapy protocol compliance (17) and is also likely to reflect lack of stratification for the most hypoxic tumors (18). Thus there is a reasonable expectation that TPZ, or an improved analog, could have a major impact on radiation therapy if developed appropriately.

Further exploration of TPZ analogs is merited because the benzotriazine di-*N*-oxide (BTO) class has two unique advantages over other bioreductive prodrugs for targeting hypoxia. Firstly, the active cytotoxin is derived from the initial free radical reduction product (19, 20), which spontaneously transforms into DNA-damaging oxidizing radicals (21, 22), while its subsequent reduction products (the 1-oxide SR4317 and nor-oxide SR4330) are much less cytotoxic (19, 23). Hypoxic selectivity of TPZ derives from the rapid reoxidation of the initial radical to the parent prodrug by O_2 (20). In contrast the active cytotoxins from other classes of bioreductive prodrugs (nitro compounds, quinones, tertiary amine *N*-oxides) are 2-,4- or 6-electron reduction products which in many cases can be generated by oxygen-insensitive two-electron reductases such as DT-diaphorase (24) or aldo-keto reductase 1C3 (25), compromising hypoxic selectivity. A second unique feature of TPZ is that it is activated under relatively mild hypoxia (26, 27); its oxygen sensitivity is approximately the inverse of that for radiotherapy, with half-maximal activation at ~ 1μM O_2 in solution (27). One-electron reduction of other bioreductive prodrugs is more sensitive to inhibition by O_2 (28–30) which restricts activation to a smaller subset of essentially anoxic cells that are arguably of lesser importance for radiation therapy (31).

These features led us to ask whether the limited clinical activity of TPZ could be improved by rational drug design. Studies with 3D cell culture models, including multicellular layers (MCL), have shown that TPZ is metabolized too rapidly to penetrate optimally into hypoxic tumor tissue (27, 32–35). We therefore hypothesized that improving the extravascular transport of TPZ would increase its therapeutic selectivity given that its penetration limitations will have a larger effect on activity in poorly perfused tumors than in well perfused normal tissues. Measurement of tissue transport parameters in MCLs has made it

possible to develop a spatially resolved pharmacokinetic/pharmacodynamic (SR-PKPD) model for TPZ, based on Green's function models of O_2 and TPZ transport, which describes its activity as a function of position within a microvascular network (36). This model has been validated as a tool for lead optimization by showing that it provides reliable prediction of activity against hypoxic cells in HT29 xenografts for a set of 16 BTOs (36). We have subsequently used the SR-PKPD model to guide lead optimization, focusing on lipophilic BTOs with potentially improved tissue diffusion coefficients (*D*) (37,38) but also holistically evaluating all other model parameters. The compounds include simple 3-amino-BTO derivatives (39, 40), 3-amino-BTOs with DNA-targeting functionality (41), 3-alkyl BTOs in which removal of the 3-amino H-bond donor usefully increases *D* (40, 42), and tricyclic triazine di-oxides (TTO) in which a lipophilic saturated ring fused to the 3-amino-BTO core also increases *D* (43). The corresponding 3-alkyl-TTO subclass (43) seeks to combine both features, and builds on experience with the BTO series (39, 42) by adjusting other physicochemical properties to optimize kinetics of bioreductive metabolism, solubility and systemic PK.

Here, we identify a 3-alkyl BTO (SN29751) and a 3-alkyl TTO (SN30000) as the preferred compounds from this SR-PKPD-guided lead optimization program. We characterize their physicochemical properties, hypoxia-selective cytotoxicity, cellular pharmacology, PK in plasma and (by modeling) in hypoxic regions of tumors. Further, we demonstrate that these novel TPZ analogs provide improved therapeutic activity against human tumor xenografts, making them potential development candidates for human therapy.

Materials and Methods

Compounds

TPZ (44) and SN29751 (45) were synthesized as reported, and SN30000 by modification[5] of a method for TTO synthesis (43). Compounds (purity > 95% by HPLC) were stored at -20°C and DMSO stock solutions at –80°C. Solubility in culture medium, octanol:water partition coefficients at pH 7.4 and mouse plasma protein binding were measured as previously (36). pK_a values were calculated using ACD/PhysChem v. 8.0 (Advanced Chemistry Development Inc., Toronto). For *in vitro* experiments DMSO stocks were diluted at least 100-fold into culture medium, while for *in vivo* studies compounds were formulated in normal saline.

Cell culture

Cell lines, from ATCC, were cultured as monolayers from *Mycoplasma*-free frozen stocks at < 3 monthly intervals in alpha minimal essential medium (αMEM) with 5% heat-inactivated fetal bovine serum (FBS) without antibiotics by weekly passage. Multicellular spheroids were grown in spinner flasks with 10% FCS and dissociated to give single cell suspensions for drug metabolism and clonogenicity assays or inoculation into mice. Multicellular layers (MCL) were grown as described (36)

In vitro growth inhibition assays

As previously (36, 39) log-phase cells were exposed to drugs for 4 h under 20% O_2 or anoxia (Bactron anaerobic chamber) and growth assessed by sulforhodamine B staining 4–5 days later. The IC_{50} was determined by nonlinear regression to the standard Hill equation and the intra-experiment hypoxic cytotoxicity ratio (HCR) calculated as aerobic IC_{50} / anoxic IC_{50}.

[5]Hay MP, Hicks KO, Pruijn FB, Pchalek K, Yang S, Blaser A, Lee HH, Siim BG, Denny WA, Wilson WR. A new class of hypoxia-selective agents with anti-tumor activity: 7,8-Dihydro-6*H*-indeno[5,6-*e*][1,2,4]triazine 1,4-dioxides. Manuscript in preparation.

In vitro drug metabolism and clonogenic cell killing

Metabolic consumption of drugs and clonogenic cell killing was measured simultaneously using magnetically-stirred single cell suspensions ($1–2\times10^6$ cells/mL) in medium without serum, equilibrated with 5% CO_2/N_2 (<100 ppm O_2) or 5% CO_2/20% O_2 as previously (35). Samples were removed at intervals, centrifuged and supernatants stored at – 80°C for HPLC. The apparent first order rate constant for drug metabolism (k_{met}) was determined from the concentration-time data by linear regression. Cell pellets were re-suspended in fresh medium, cell number determined by Coulter counter and viability by 0.4% trypan blue exclusion. Cells were plated to determine clonogenic survival. The data were fitted using the previous (36) cellular PKPD model in which the rate of log cell kill (LCK, defined as the negative log of the surviving fraction SF) at time t is proportional to both the rate of drug metabolism and the parent drug concentration C:

$$\frac{d\log SF}{dt}=\gamma C\frac{dM}{dt} \quad \text{(Eqn 1)}$$

where $dM/dt = k_{met} \times C/\phi$ is the metabolized drug per unit cell volume, ϕ is the HT29 cell volume fraction determined from the cell count as previously (35), γ is the proportionality constant and C_0 is the initial measured drug concentration. To allow for decreasing drug concentrations during exposure, Eqn 1 was integrated to give

$$-\log SF=\gamma E \quad \text{(Eqn 2)}$$

where the "exposure integral" E, at each sampling time, t, is given by:

$$E=\frac{C_0^2}{2\phi}\left[1-e^{-2\phi k_{met}T}\right] \quad \text{(Eqn 3)}$$

E was plotted against log SF to obtain the potency coefficient γ by regression as previously validated for TPZ (35) and TPZ analogs (36).

Oxygen dependence of cytotoxicity *in vitro*

Clonogenic cell killing was measured over a range of oxygen concentrations in stirred cell suspensions as previously (27), using lower cell densities (3×10^5 cells/mL) to minimise the effect of cellular respiration on solution oxygen concentrations (C_s), which were monitored using an OxyLite 2000 O_2 luminescent probe (Oxford Optronix Ltd). Drug concentrations were also monitored, 30–60 min intervals, by HPLC and the cell survival data were fitted as above. The potency as a function of C_s was fitted to a Hill equation to estimate K_{O2} (C_s to halve anoxic potency) by regression.

Diffusion in multicellular layers

Diffusion through HT29 and SiHa MCL was determined as previously (36, 37) using a 2-chamber diffusion apparatus (46). The medium was equilibrated with 95% O_2 to suppress bioreductive metabolism. Compounds were added to the donor compartments with ^{14}C-urea and samples taken at intervals to assay drug (by HPLC) and ^{14}C-urea (liquid scintillation counting) in both compartments. MCL thicknesses and drug diffusion coefficients (D_{mcl}) were fitted to the concentration-time profiles of urea and drug respectively, using a Fick's Second Law mathematical model (36).

High-performance liquid chromatography

Drug concentrations were determined with a 150mm × 2.1mm Alltima C8 reverse phase column and Agilent 1100 HPLC using photodiode array detection. For *in vitro* studies,

culture supernatants were analyzed by direct injection (35). Plasma samples (below) were analyzed following previous methods (36) after precipitation of proteins with acetonitrile, evaporation to dryness in a Speed-Vac concentrator and reconstitution in 125 μL of 45 mM ammonium formate buffer pH 4.5, of which 100 μL was injected.

Animal toxicity

All animal experiments followed institutional protocols as previously (36). Specific pathogen free CD-1 nu/nu mice (~ 25 g) or Sprague-Dawley rats (~ 200 g) were ear-tagged and randomized to treatment groups. Freshly prepared solutions of compounds were administered intraperitoneally (i.p.) to mice at 20 mL/kg body weight, or to rats at 10 mL/kg (25 mL/kg for TPZ), using 1.33-fold dose increments. The maximum tolerated dose (MTD) was defined as the highest dose that caused no drug-related deaths, body weight loss of more than 15%, or severe morbidity in a group of three to six animals, with an observation time of 28 days.

Plasma pharmacokinetics

Mice were injected i.p. or i.v. at 75 % of the MTD for each compound, with sampling by cardiac puncture under terminal CO_2 anesthesia. Rats were injected i.p. at 178 and 316 μmol/kg and blood samples of 20–40 μL obtained serially from the saphenous vein without anesthesia. Blood was immediately centrifuged (3,000 *g*, 3min) and plasma stored at –80°C for HPLC. Non-compartmental PK parameters were determined by WinNonLin v 5 (Pharsight Corp.).

Xenograft models

Tumor xenografts were grown s.c. in the dorsal flank of CD-1 nude mice, 1.5 cm from the base of the tail, by inoculation of 10^7 cells. Treatment was initiated when tumors reached a mean diameter of 9–11 mm, using i.p. dosing with either a single dose or multi-dose (bi-daily at 9 am and 3 pm for consecutive 4 days) schedule, at various times before or after irradiation. Mice were irradiated without anesthesia using a cobalt-60 gamma source, either whole-body (15 or 20 Gy) for single dose studies or locally using a custom-built restraining jig for multidose studies (2 or 2.5 Gy×8). Tumor response was assessed by clonogenic assay of cell suspensions from xenografts removed 18 h after the end of treatment (excision assay) as previously (36). Log cell kill (LCK) was calculated from the difference in log clonogens/g for treated and control groups. Statistical significance of drug effects was tested using one way ANOVA with Dunnett's test for multiple comparisons. Alternatively, tumors were measured 3×weekly using callipers until tumors reached 3×pre-treatment volume (regrowth assay).

Spatially resolved PKPD modeling

Oxygen and drug concentration gradients were calculated using the Green's function method in a mapped microvascular network (500×500×230 μm) from a rat R3230Ac tumor as previously (36), based on the tissue diffusion coefficients and rate constants for drug metabolism measured *in vitro* above with inflow drug concentration defined by the measured plasma PK. Drug-induced cell kill at each point in the tumor microregion was then calculated using the above cellular PKPD model. Radiation-induced cell kill at each point was also calculated, using reported linear-quadratic model parameters (36). The predicted surviving fraction (SF) for drug and radiation was averaged over the whole tumor microregion to calculate the overall log cell kill (LCK). The difference between SF for drug with radiation and radiation alone gave the predicted drug-induced LCK in the radiation-resistant hypoxic cell population.

Results

PKPD-guided lead optimization

An overview of the algorithm we used to identify improved TPZ analogs is shown in Fig. 1A. Of 281 BTO and TTO compounds synthesized from 5 different structural classes, 225 had sufficient solubility to determine hypoxia-selective cytotoxicity in IC_{50} assays. 182 passed decision point 'A' in Fig. 1A (HCR > 20 against both HT29 and SiHa cells), and 173 of these were evaluated in additional tissue culture models to determine the parameters required for SR-PKPD modeling. This included measurement of clonogenic cell killing and metabolic drug consumption under anoxia (first order rate constant $k_{met,0}$) in stirred HT29 cell suspensions. We also calculated tumor tissue diffusion coefficients (D) from physicochemical parameters (MW, logP at pH 7, hydrogen bond donors and acceptors) using relationships previously established with a training set of BTOs in 3D multicellular layer (MCL) cultures (38). The range of values of $k_{met,0}$ and D are shown in Fig. 1B, which illustrates the diversity of extravascular transport properties; compounds lying below the diagonal line are predicted to have superior penetration distances into hypoxic HT29 tissue relative to TPZ (40).

A first iteration of the SR-PKPD model was then run to predict the hypoxic cytotoxicity differential (HCD = LCK in the radiobiologically hypoxic region [< 4 μM O_2]/aerobic region [>30 μM O_2]) of each compound in HT29 xenografts and the plasma AUC required for a hypoxic LCK of >0.5. Compounds passed this decision point ('B' in Fig. 1A) if HCD >1 and the required AUC was <333 μM-h, which is twice that of TPZ at its MTD in initial PK studies in this mouse strain (36). For 115 compounds, we determined the MTD in CD-1 nude mice and the plasma AUC at 75% of MTD. The SR-PKPD model was then re-run using the measured AUC to identify compounds with LCK > 0.3 at 75% MTD. Compounds passing this third decision point ('C' in Fig. 1A) were then evaluated *in vivo* by testing their ability to kill radiation-resistant hypoxic cells in HT29 xenografts following a single drug dose at 75% of MTD. Sixteen of the 18 compounds predicted to be active showed statistically significant activity, while a further 12 compounds predicted to be inactive were also tested to evaluate the algorithm and were all found to be inactive. SN29751 was identified as the most promising of the BTO series (42), and SN30000 as the preferred analog in the new TTO series5. The structures of these lead candidates are shown in Fig. 1C, along with their stable 2e reduction products (1-oxides 1 and 2). These new analogs showed ≥ 5-fold higher aqueous solubility than TPZ despite increased lipophilicity at neutral pH (Table 1).

Bioreductive metabolism and cytotoxicity of SN29751 and SN30000

A more detailed investigation of each component of the pharmacology of these new lead compounds was undertaken. The metabolism of the prodrugs in HT29 cultures, illustrated in Fig. 1D, demonstrated hypoxia-dependent loss of the parent compounds with formation of the 1-oxides (and for SN30000 a trace of the nor-oxide 3) identified by comparison of retention time and absorbance spectra with authentic standards (Fig. S1). Over all experiments, the rate constant for bioreductive consumption ($k_{met,0}$) was highest for SN30000 (1.53 ± 0.21 min^{-1}; errors are SEM throughout), intermediate for TPZ (1.30 ± 0.04 min^{-1}) and lowest for SN29751 (0.87 ± 0.03 min^{-1}).

SN29751 and SN30000, like TPZ, showed hypoxia-selective cytotoxicity in HT29 and SiHa IC_{50} (anti-proliferative) assays, while the reduced metabolites were substantially less cytotoxic and lacked hypoxic selectivity (Fig. 2A). Extending this assay to 8 cell lines, SN30000 was consistently more potent than TPZ under anoxia while SN29751 was less potent (Fig. 2B). Notably, anoxic potency of both compounds was highly correlated with

that of TPZ across the cell lines (Fig. 2B; R^2 = 0.97 and 0.93 for SN29751 and SN30000 respectively), suggesting a common mechanism of action. Consistent with its higher potency under anoxia, the HCR was consistently higher for SN30000 than TPZ and SN29751 across all cell lines (Fig. 2C). These findings were confirmed for HT29 cells by clonogenic assay (Fig. 2D), which showed highest anoxic potency (coefficient γ in Table 1) and HCR values for SN30000.

Penetration of multicellular layer cultures

Diffusion coefficients of SN30000 and SN29751 in HT29 MCL, calculated from their physicochemical properties, were higher than for TPZ (Fig. 1B). These predictions were confirmed by measuring penetration through aerobic HT29 MCL (Fig 3A). At these high oxygen concentrations, no reduced metabolites were observed and diffusion coefficients (D_{MCL}) could be fitted as simple diffusion without metabolism (Fig. 3B); the values for SN30000 and SN29751 were 3-fold and 2.5-fold higher, respectively, than TPZ (Table 1). This same trend (SN30000 > SN29751 > TPZ) was seen in SiHa MCL (Fig. S2)

Oxygen dependence of cytotoxicity and metabolism

We defined the oxygen dependence of SN29751 and SN30000 activation using the same approach as previously (27), thus testing the assumption in the initial SR-PKPD screen (Fig. 1A) that this was the same as for TPZ. As illustrated for SN30000 (Fig. 3C), the slope of the survival vs exposure integral plots decreased with increasing oxygen concentration in solution. These slopes were used to determine cytotoxic potency as a function of oxygen (Fig. 3D). The oxygen concentration required to halve the anoxic potency of SN30000 and SN29751 (K_{O2} ~ 1 μM, Table 1) was not significantly different (one way ANOVA, p=0.26) from that for TPZ. Metabolic consumption of the prodrugs, in the same experiments, showed similar oxygen dependence (Fig. S3) with 50% inhibition at ~ 0.6–1 μM O_2.

Toxicity and plasma pharmacokinetics in mice and rats

Following single i.p. administration, the maximum tolerated dose (MTD) in male CD-1 nude mice was 1000 μmol/kg (370 mg/kg) for SN29751 and 750 μmol/kg (275 mg/kg) for SN30000, i.e. 5.6-fold and 4.2-fold respectively higher molar doses than for TPZ (178 μmol/kg, 31.7 mg/kg). As summarized in Table S1, these differences in host toxicity (SN29751 < SN30000 < TPZ) were also seen in the three other mouse strains investigated (C3H/HeN, C57/Bl6, Rag-$1^{-/-}$) and with other dosing schedules in CD-1 nude mice. For example, the MTD for bi-daily dosing (9 am and 3 pm) for 4 consecutive days (BID1-4) was 421 μmol/kg for SN29751, 237 μmol/kg for SN30000 and 75 μmol/kg for TPZ.

Histopathology of CD-1 nude mice following single drug doses or the BID1-4 schedule at 1–1.3×MTD showed a qualitatively similar organ toxicity profile for SN29751, SN30000 and TPZ (Table S2). For single doses, bone marrow hypoplasia, gastrointestinal toxicity and airway epithelium vacuolation were the most pronounced acute findings. Following the BID1-4 schedule, histopathological changes were similar to the single dose study for SN29751, but gastrointestinal toxicity was the only acute finding for SN30000 and TPZ. As reported previously for TPZ in mice (47), significant retinal toxicity was observed 28 days after treatment by all three agents (Fig. S4).

Initial screening of PK following single i.p. doses at 75% MTD in CD-1 nude mice (Fig. 4A) indicated similar plasma half lives of all three compounds (28, 35 and 32 min for TPZ, SN29751 and SN30000 respectively; Table 1). However, increased plasma concentrations were achieved for the analogs resulting in AUC values of 49, 162, 79 μM.h for TPZ, SN29751 and SN30000 respectively at these equitoxic doses (Table 1). Comparison with i.v. dosing demonstrated an i.p. bioavailability of 77% for SN30000 (Table S3).

Comparison of toxicity and plasma PK in Sprague-Dawley rats again demonstrated higher MTD values for the analogs (178 μmol/kg for TPZ and 316 μmol/kg for SN30000 in both sexes, 316 μmol/kg for SN29751 in females and 421 μmol/kg in males) after single i.p. doses. Representative plasma PK is shown in Fig 4B; C_{max}, terminal half lives and AUC (Table S4) were all higher for the analogs than TPZ.

SR-PKPD modeling of tumor cell killing in combination with radiation

The measured parameters of the SR-PKPD model, summarized in Table 1, allow a complete description of PK and PD (cell killing) at each point within HT29 xenografts; the model output is shown in Fig. 4C for all three compounds at 75% of MTD in CD-1 nude mice. The model predicts a large increase in hypoxic cell killing by SN30000 and SN29751 relative to TPZ at equivalent host toxicity. In both cases killing shows excellent complementarity to that calculated for a large single dose of radiation (20 Gy), which spares the hypoxic cells (dashed line in Fig. 4C). To model overall log cell kill (LCK) by each drug when used in combination with radiation we assumed independent action of both agents and summed all tissue regions for the combination, subtracting LCK for radiation alone. This additional LCK, and the model-predicted hypoxic selectivity (HCD) both showed a clear increase for SN30000 and SN29751 relative to TPZ at equivalent host toxicity (Fig. 4D). We also simulated the activity of the compounds against an HT29 tumor notionally grown in Sprague-Dawley rats, based on the measured plasma PK at MTD. The spatially resolved PD predictions (Fig. S5) again show a large improvement in hypoxic cell killing for the analogs relative to TPZ at equivalent host toxicity, and the combined activity with radiation for this “virtual therapeutic trial” (Fig. 4D) is again predicted to be markedly superior to TPZ.

Activity against human tumor xenografts

The SR-PKPD model predictions were in good agreement with the measured killing of HT29 cells in xenografts by excision assay (Fig. 5A), which showed greater LCK for SN30000 and SN29751 than TPZ when administered at 75% of MTD 5 min after a single dose of radiation (to sterilize well oxygenated cells). A similar large (~3-fold) increase in hypoxic tumor cell killing was seen with SiHa and H460 xenografts (Fig. 5A). No significant activity was seen with the drugs alone (without radiation) against any of the xenografts, consistent with selective killing of the hypoxic subpopulation (data not shown). The analogs were also generally superior to TPZ when administered 30 min before each fraction of a BID1-4 radiotherapy schedule (Fig. 5A). The time course of interaction between the drugs and radiation against SiHa tumors (Fig. 5B) also demonstrated higher activity of SN29751 and SN30000 and showed that the compounds were active both before and after irradiation, as for TPZ, demonstrating that the mechanism is hypoxic cell killing rather than direct radiosensitization.

Activity of SN30000 with fractionated radiation was also evaluated in SiHa tumors using tumor regrowth as the endpoint (Fig. 5C), demonstrating significant activity additional to radiation at the two highest drug doses tested. Comparison with TPZ in the same experiment is shown in Fig. 5D, where the time for tumor regrowth is compared with body weight loss (as a measure of toxicity). Both TPZ and SN30000 showed dose-dependent body weight loss and inhibition of tumor regrowth, but with greater antitumor activity for SN30000 relative to toxicity.

Discussion

This study identifies novel TPZ analogs with improved formulation properties (aqueous solubility), cytotoxic potency against hypoxic cells in culture, tissue penetration characteristics and therapeutic activity against hypoxic cells in multiple tumor models.

Perhaps most notably, the approach we have taken represents a departure from the usual strategy for lead optimization during anticancer drug development in which potency and selectivity in monolayer cell cultures is used to select compounds for evaluation in *in vivo* models. In contrast, we use spatially resolved (SR)-PKPD modeling to make a holistic assessment of the molecular features that contribute to antitumor activity *in vivo*. The SR-PKPD model for TPZ analogs incorporates the relationships between prodrug metabolism, cytotoxicity and oxygen concentration as determined *in vitro*, the systemic (plasma) pharmacokinetics of the compounds at tolerated doses, and their extravascular transport (tissue penetration) in tumors as assessed with the MCL model. The latter aspect enables calculation of drug concentration gradients in a representative microvascular network, and thus prediction of cell killing probability at each position in the tumor tissue.

The utility of this SR-PKPD approach is demonstrated by confirmed hypoxia-selective cell killing in HT29 xenografts for 16 of 18 compounds predicted by the model to be active (one of the 2 false positives showed a hypoxic LCK of 0.60 ± 0.36, which did not reach statistical significance), and the quantitative agreement between model prediction and measured hypoxic cell killing in HT29 xenografts for TPZ, SN29751 and SN30000 (compare left panels of Fig. 4A and Fig. 5A). In contrast, 12/12 compounds predicted by the SR-PKPD model to be inactive (despite good hypoxic selectivity *in vitro*) were confirmed as true negatives. This suggests that the assumptions adopted in the modeling are acceptable for this drug series, including that the microvascular geometry of the rat 3230Ac tumor (used as the basis for our Green's function oxygen and drug transport model) is representative of human tumor xenografts, and that the intrinsic sensitivity of HT29 cells is the same in single cell culture and tumors.

Notably, the inactive compounds *in vivo* showed hypoxic potency and selectivity for HT29 cells in culture in the same range as for the active compounds, and linear regression showed that neither hypoxic potency (IC_{50}; $r^2 = 0.07$, p=0.16) nor selectivity ($log_{10}HCR$; $r^2 = 0.02$, p = 0.47) *in vitro* correlated with hypoxic LCK in tumors (Fig. S6). Thus the key determinants of therapeutic activity are systemic PK relative to toxicity, and intratumor PK (consistent with evidence that this is a limiting feature for TPZ itself (32))(27, 33–36); these features are explicitly represented in the model. In the case of SN30000, the improvement over TPZ is mainly driven by its superior extravascular penetration (Fig. 3B, Fig. S2) and higher cytotoxic potency under hypoxia (Fig. 2B,C,D), while for SN29751 improved systemic (plasma) PK (Fig. 4A) makes a larger contribution to its higher activity against xenografts in mice. The improved extravascular penetration of SN30000 is consistent with its higher lipophilicity (Table 1) and removal of the H-bond donor 3-NH_2 group, these features being the major determinants of MCL diffusion coefficients for TPZ analogs (38). The higher hypoxic cytotoxicity potency of SN30000 presumably reflects its 57 mV higher one-electron reduction potential5 and consequent faster bioreductive metabolism (Fig. 1D and Table 1). In effect, the higher diffusion coefficient of SN30000 permits faster bioreductive activation without compromising penetration into the hypoxic target zone.

Studies with three xenograft models demonstrate a substantial (ca 3-fold) therapeutic gain for SN30000 and SN29751 over TPZ with single dose radiation (Fig. 5A), and SR-PKPD model predictions based on plasma PK achievable in rats also indicate a large therapeutic advantage for the analogs over TPZ in this second species (Fig. 4D). SN30000 and SN29751 are also clearly superior to TPZ in combination with fractionated radiation (Fig. 5A,B,D), although the magnitude of improvement with HT29 tumors appears to be less than for single dose radiation (Fig. 5A). This might reflect a lesser penetration problem for bioreductive prodrugs in combination with fractionated radiation if, as suggested (31), moderately hypoxic cells closer to blood vessels make a larger contribution to outcome than severely hypoxic cells in this setting.

The present study demonstrates that the mechanism of action of SN30000 and SN29751 is similar to that of TPZ. All three compounds are metabolised under hypoxia to the corresponding non-toxic 1-oxides (Fig. 1D), with an indistinguishable cell line dependence as hypoxic cytotoxins (Fig. 2B). Consistent with this, we have recently shown a strong correlation between TPZ and SN30000 reductive metabolism under hypoxia in a panel of 16 cell lines (48). In addition, the relationship between γH2AX formation and clonogenic cell killing is the same for TPZ, SN30000 and SN29751, and CHO cell lines defective in homologous recombination repair show similar hypersensitivity to all three compounds (unpublished data), consistent with cytotoxicity of the new analogs occurring via replication fork arrest as for TPZ (49). Coupled with the similar oxygen dependence of the three agents in HT29 cultures (Fig. 3D and Fig. S3) and similar normal tissue histopathology in mice (Table S2), these observations suggest that SN30000 and SN29751 are well positioned to leverage clinical experience with TPZ including the use of PET imaging to prospectively identify hypoxic tumors (18).

PK evaluation of anticancer drugs during clinical development is typically limited to describing concentration-time profiles in plasma, rather than in the effect compartment within tumors. The spatially resolved PK model described here provides a unique opportunity to simulate PK in hypoxic regions of tumors during phase I trial of SN30000, and to compare this with an analogous simulation for TPZ based on its reported plasma at MTD in humans (50). We plan to link this to PD prediction in humans using the cellular PKPD model described here, essentially as for the “virtual therapeutic trial” in rats represented by Fig. 4D. This will provide an early indication, independent of response biomarkers, whether SN30000 offers a therapeutic gain over TPZ as a hypoxic cytotoxin for use in humans.

Supplementary Material

Refer to Web version on PubMed Central for supplementary material.

Acknowledgments

We thank Dianne Ferry for assistance with bioanalysis, and Drs Jingli Wang and Thorsten Melcher for critical comments on the manuscript.

Grant support: This study was funded by grants from the US National Institutes of Health (CA82566), the Cancer Society of New Zealand (CSNZ05/17) and Proacta Therapeutics Ltd.

References

1. Pries AR, Cornelissen AJ, Sloot AA, Hinkeldey M, Dreher MR, Höpfner M, et al. Structural adaptation and heterogeneity of normal and tumor microvascular networks. PLoS computational biology. 2009; 5 e1000394.
2. Wardman P. The importance of radiation chemistry to radiation and free radical biology. (The 2008 Silvanus Thompson Memorial Lecture). Br J Radiol. 2009; 82:89–104. [PubMed: 19168690]
3. Lunt SJ, Chaudary N, Hill RP. The tumor microenvironment and metastatic disease. Clin Expl Metast. 2009; 26:19–34.
4. Brizel DM, Scully SP, Harrelson JM, Layfield LJ, Bean JM, Prosnitz LR, et al. Tumor oxygenation predicts for the likelihood of distant metastases in human soft tissue sarcoma. Cancer Res. 1996; 56:941–943. [PubMed: 8640781]
5. Fyles A, Milosevic M, Hedley D, Pintilie M, Levin W, Manchul L, et al. Tumor hypoxia has independent predictor impact only in patients with node-negative cervix cancer. J Clin Oncol. 2002; 20:680–687. [PubMed: 11821448]

6. Rofstad EK, Mathiesen B, Henriksen K, Kindem K, Galappathi K. The tumor bed effect: increased metastatic dissemination from hypoxia-induced up-regulation of metastasis-promoting gene products. Cancer Res. 2005; 65:2387–2396. [PubMed: 15781654]
7. Kioi M, Vogel H, Schultz G, Hoffman RM, Harsh GR, Brown JM. Inhibition of vasculogenesis, but not angiogenesis, prevents the recurrence of glioblastoma after irradiation in mice. J Clin Invest. 2010; 120:694–705. [PubMed: 20179352]
8. Vaupel P, Hockel M, Mayer A. Detection and characterization of tumor hypoxia using pO2 histography. Antioxid Redox Signal. 2007; 9:1221–1235. [PubMed: 17536958]
9. Semenza GL. Defining the role of hypoxia-inducible factor 1 in cancer biology and therapeutics. Oncogene. 2010; 29:625–634. [PubMed: 19946328]
10. Rouschop KM, van den BT, Dubois L, Niessen H, Bussink J, Savelkouls K, et al. The unfolded protein response protects human tumor cells during hypoxia through regulation of the autophagy genes MAP1LC3B and ATG5. J Clin Invest. 2010; 120:127–141. [PubMed: 20038797]
11. Brown JM, Wilson WR. Exploiting tumor hypoxia in cancer treatment. Nat Rev Cancer. 2004; 4:437–447. [PubMed: 15170446]
12. McKeown SR, Cowen RL, Williams KJ. Bioreductive drugs: from concept to clinic. Clin Oncol. 2007; 19:427–442.
13. Chen Y, Hu L. Design of anticancer prodrugs for reductive activation. Med Res Rev. 2009; 29:29–64. [PubMed: 18688784]
14. von Pawel J, von Roemeling R, Gatzemeier U, Boyer M, Elisson LO, Clark P, et al. Tirapazamine plus cisplatin versus cisplatin in advanced non-small-cell lung cancer: A report of the international CATAPULT I study group. Cisplatin and Tirapazamine in Subjects with Advanced Previously Untreated Non-Small-Cell Lung Tumors. J Clin Oncol. 2000; 18:1351–1359. [PubMed: 10715308]
15. Rischin D, Peters L, Fisher R, Macann A, Denham J, Poulsen M, et al. Tirapazamine, cisplatin, and radiation versus fluorouracil, cisplatin, and radiation in patients with locally advanced head and neck cancer: a randomized phase II trial of the Trans-Tasman Radiation Oncology Group (TROG 98.02). J Clin Oncol. 2005; 23:79–87. [PubMed: 15625362]
16. Rischin D, Peters LJ, O'Sullivan B, Giralt J, Fisher R, Yuen K, et al. Tirapazamine, cisplatin, and radiation versus cisplatin and radiation for advanced squamous cell carcinoma of the head and neck (TROG 02.02, HeadSTART): A phase III trial of the Trans-Tasman Radiation Oncology Group. J Clin Oncol. 2010
17. Peters LJ, O'Sullivan B, Giralt J, Fitzgerald TJ, Trotti A, Bernier J, et al. Critical impact of radiotherapy protocol compliance and quality in the treatment of advanced head and neck cancer: Results from TROG 02.02. J Clin Oncol. 2010
18. Rischin D, Hicks RJ, Fisher R, Binns D, Corry J, Porceddu S, et al. Prognostic significance of [18F]-misonidazole positron emission tomography-detected tumor hypoxia in patients with advanced head and neck cancer randomly assigned to chemoradiation with or without tirapazamine: a substudy of Trans-Tasman Radiation Oncology Group Study 98.02. J Clin Oncol. 2006; 24:2098–2104. [PubMed: 16648512]
19. Baker MA, Zeman EM, Hirst VK, Brown JM. Metabolism of SR 4233 by Chinese hamster ovary cells: basis of selective hypoxic cytotoxicity. Cancer Res. 1988; 48:5947–5952. [PubMed: 3167847]
20. Laderoute K, Wardman P, Rauth AM. Molecular mechanisms for the hypoxia-dependent activation of 3-amino- 1,2,4-benzotriazine-1,4-dioxide (SR 4233). Biochem Pharmacol. 1988; 37:1487–1495. [PubMed: 3128984]
21. Junnotula V, Sarkar U, Sinha S, Gates KS. Initiation of DNA strand cleavage by 1,2,4-benzotriazine 1,4-dioxide antitumor agents: mechanistic insight from studies of 3-methyl-1,2,4-benzotriazine 1,4-dioxide. J Am Chem Soc. 2009; 131:1015–1024. [PubMed: 19117394]
22. Shinde SS, Maroz A, Hay MP, Patterson AV, Denny WA, Anderson RF. Characterization of radicals formed following enzymatic reduction of 3-substituted analogues of the hypoxia-selective cytotoxin 3-amino-1,2,4-benzotriazine 1,4-dioxide (tirapazamine). J Am Chem Soc. 2010; 132:2591–2599. [PubMed: 20141134]

23. Siim BG, Pruijn FB, Sturman JR, Hogg A, Hay MP, Brown JM, et al. Selective potentiation of the hypoxic cytotoxicity of tirapazamine by its 1-N-oxide metabolite SR 4317. Cancer Res. 2004; 64:736–742. [PubMed: 14744792]
24. Knox RJ, Chen S. Quinone reductase-mediated nitro-reduction: clinical applications. Methods Enzymol. 2004; 382:194–221. [PubMed: 15047103]
25. Guise CP, Abbattista M, Singleton RS, Holford SD, Connolly J, Dachs GU, et al. The bioreductive prodrug PR-104A is activated under aerobic conditions by human aldo-keto reductase 1C3. Cancer Res. 2010; 70:1573–1584. [PubMed: 20145130]
26. Koch CJ. Unusual oxygen concentration dependence of toxicity of SR-4233, a hypoxic cell toxin. Cancer Res. 1993; 53:3992–3997. [PubMed: 8358728]
27. Hicks KO, Siim BG, Pruijn FB, Wilson WR. Oxygen dependence of the metabolic activation and cytotoxicity of tirapazamine: implications for extravascular transport and activity in tumors. Radiat Res. 2004; 161:656–666. [PubMed: 15161354]
28. Marshall RS, Rauth AM. Oxygen and exposure kinetics as factors influencing the cytotoxicity of porfiromycin, a mitomycin C analogue, in Chinese hamster ovary cells. Cancer Res. 1988; 48:5655–5659. [PubMed: 3167822]
29. Siim BG, Atwell GJ, Wilson WR. Oxygen dependence of the cytotoxicity and metabolic activation of 4- alkylamino-5-nitroquinoline bioreductive drugs. Br J Cancer. 1994; 70:596–603. [PubMed: 7917903]
30. Hicks KO, Myint H, Patterson AV, Pruijn FB, Siim BG, Patel K, et al. Oxygen dependence and extravascular transport of hypoxia-activated prodrugs: comparison of the dinitrobenzamide mustard PR-104A and tirapazamine. Int J Radiat Oncol Biol Phys. 2007; 69:560–571. [PubMed: 17869669]
31. Wouters BG, Brown JM. Cells at intermediate oxygen levels can be more important than the "hypoxic fraction" in determining tumor response to fractionated radiotherapy. Radiat Res. 1997; 147:541–550. [PubMed: 9146699]
32. Durand RE, Olive PL. Physiologic and cytotoxic effects of tirapazamine in tumor-bearing mice. Radiat Oncol Investig. 1997; 5:213–219.
33. Hicks KO, Fleming Y, Siim BG, Koch CJ, Wilson WR. Extravascular diffusion of tirapazamine: effect of metabolic consumption assessed using the multicellular layer model. Int J Radiat Oncol Biol Phys. 1998; 42:641–649. [PubMed: 9806526]
34. Kyle AH, Minchinton AI. Measurement of delivery and metabolism of tirapazamine to tumour tissue using the multilayered cell culture model. Cancer Chemother Pharmacol. 1999; 43:213–220. [PubMed: 9923551]
35. Hicks KO, Pruijn FB, Sturman JR, Denny WA, Wilson WR. Multicellular resistance to tirapazamine is due to restricted extravascular transport: a pharmacokinetic/pharmacodynamic study in HT29 multicellular layer cultures. Cancer Res. 2003; 63:5970–5977. [PubMed: 14522924]
36. Hicks KO, Pruijn FB, Secomb TW, Hay MP, Hsu R, Brown JM, et al. Use of three-dimensional tissue cultures to model extravascular transport and predict in vivo activity of hypoxia-targeted anticancer drugs. J Natl Cancer Inst. 2006; 98:1118–1128. [PubMed: 16912264]
37. Pruijn FB, Sturman JR, Liyanage HDS, Hicks KO, Hay MP, Wilson WR. Extravascular transport of drugs in tumor tissue: Effect of lipophilicity on diffusion of tirapazamine analogs in multicellular layer cultures. J Med Chem. 2005; 48:1079–1087. [PubMed: 15715475]
38. Pruijn FB, Patel K, Hay MP, Wilson WR, Hicks KO. Prediction of tumour tissue diffusion coefficients of hypoxia-activated prodrugs from physicochemical parameters. Aust J Chem. 2008; 61:687–693.
39. Hay MP, Gamage SA, Kovacs MS, Pruijn FB, Anderson RF, Patterson AV, et al. Structure-activity relationships of 1,2,4-benzotriazine 1,4-dioxides as hypoxia-selective analogues of tirapazamine. J Med Chem. 2003; 46:169–182. [PubMed: 12502371]
40. Hay MP, Hicks KO, Pruijn FB, Pchalek K, Siim BG, Wilson WR, et al. Pharmacokinetic/pharmacodynamic model-guided identification of hypoxia-selective 1,2,4-benzotriazine 1,4-dioxides with antitumor activity: the role of extravascular transport. J Med Chem. 2007; 50:6392–6404. [PubMed: 18001018]

41. Hay MP, Pruijn FB, Gamage SA, Liyanage HD, Kovacs MS, Patterson AV, et al. DNA-Targeted 1,2,4-Benzotriazine 1,4-Dioxides: Potent Analogues of the Hypoxia-Selective Cytotoxin Tirapazamine. J Med Chem. 2004; 47:475–488. [PubMed: 14711317]
42. Hay MP, Pchalek K, Pruijn FB, Hicks KO, Siim BG, Anderson RF, et al. Hypoxia-selective 3-alkyl 1,2,4-benzotriazine 1,4-dioxides: the influence of hydrogen bond donors on extravascular transport and antitumor activity. J Med Chem. 2007; 50:6654–6664. [PubMed: 18052317]
43. Hay MP, Hicks KO, Pchalek K, Lee HH, Blaser A, Pruijn FB, et al. Tricyclic [1,2,4]triazine 1,4-dioxides as hypoxia selective cytotoxins. J Med Chem. 2008; 51:6853–6568. [PubMed: 18847185]
44. Boyd M, Hay MP, Boyd PD. Complete ^{1}H, ^{13}C and ^{15}N NMR assignment of tirapazamine and related 1,2,4-benzotriazine N-oxides. Magn Reson Chem. 2006; 44:948–954. [PubMed: 16900565]
45. Pchalek K, Hay MP. Stille coupling reactions in the synthesis of hypoxia-selective 3-alkyl-1,2,4-benzotriazine 1,4-dioxide anticancer agents. J Org Chem. 2006; 71:6530–6535. [PubMed: 16901140]
46. Hicks KO, Pruijn FB, Baguley BC, Wilson WR. Extravascular transport of the DNA intercalator and topoisomerase poison *N*-[2-(dimethylamino)ethyl]acridine-4-carboxamide (DACA): diffusion and metabolism in multicellular layers of tumor cells. J Pharmacol Exp Ther. 2001; 297:1088–1098. [PubMed: 11356933]
47. Lee AE, Wilson WR. Hypoxia-dependent retinal toxicity of bioreductive anticancer prodrugs in mice. Toxicol Appl Pharmacol. 2000; 163:50–59. [PubMed: 10662604]
48. Wang J, Ferry D, Hay MP, Patel R, Koch CJ, Wilson WR. Comparison of bioreductive metabolism of tirapazamine, its second generation analogue SN 30000 and hypoxia imaging agent EF5 in human tumor cell lines. Proc Am Assoc Cancer Res. 2010 abstract 2282.
49. Evans JW, Chernikova SB, Kachnic LA, Banath JP, Sordet O, Delahoussaye YM, et al. Homologous recombination is the principal pathway for the repair of DNA damage induced by tirapazamine in mammalian cells. Cancer Res. 2008; 68:257–265. [PubMed: 18172318]
50. Senan S, Rampling R, Graham MA, Wilson P, Robin H Jr, Eckardt N, et al. Phase I and pharmacokinetic study of tirapazamine (SR 4233) administered every three weeks. Clin Cancer Res. 1997; 3:31–38. [PubMed: 9815534]

Statement of translational relevance

Hypoxia is a ubiquitous feature of tumors and arguably one of the most important therapeutic targets in oncology which has yet to be exploited. Tirapazamine (TPZ) is the best-studied hypoxia-activated prodrug, but has limited clinical activity in part because of inefficient penetration into hypoxic tumor tissue. We have used a novel spatially resolved pharmacokinetic/pharmacodynamic (SR-PKPD) modeling approach to guide optimization of TPZ analogs for improved tissue penetration and hypoxic cell killing in tumors. The resulting compounds, SN29751 and SN30000, show clear improvement over TPZ in therapeutic activity in multiple xenograft models in combination with either single dose or fractionated radiation. The SR-PKPD tools developed in this study will assist in the clinical development of SN30000 as a hypoxia-targeted prodrug.

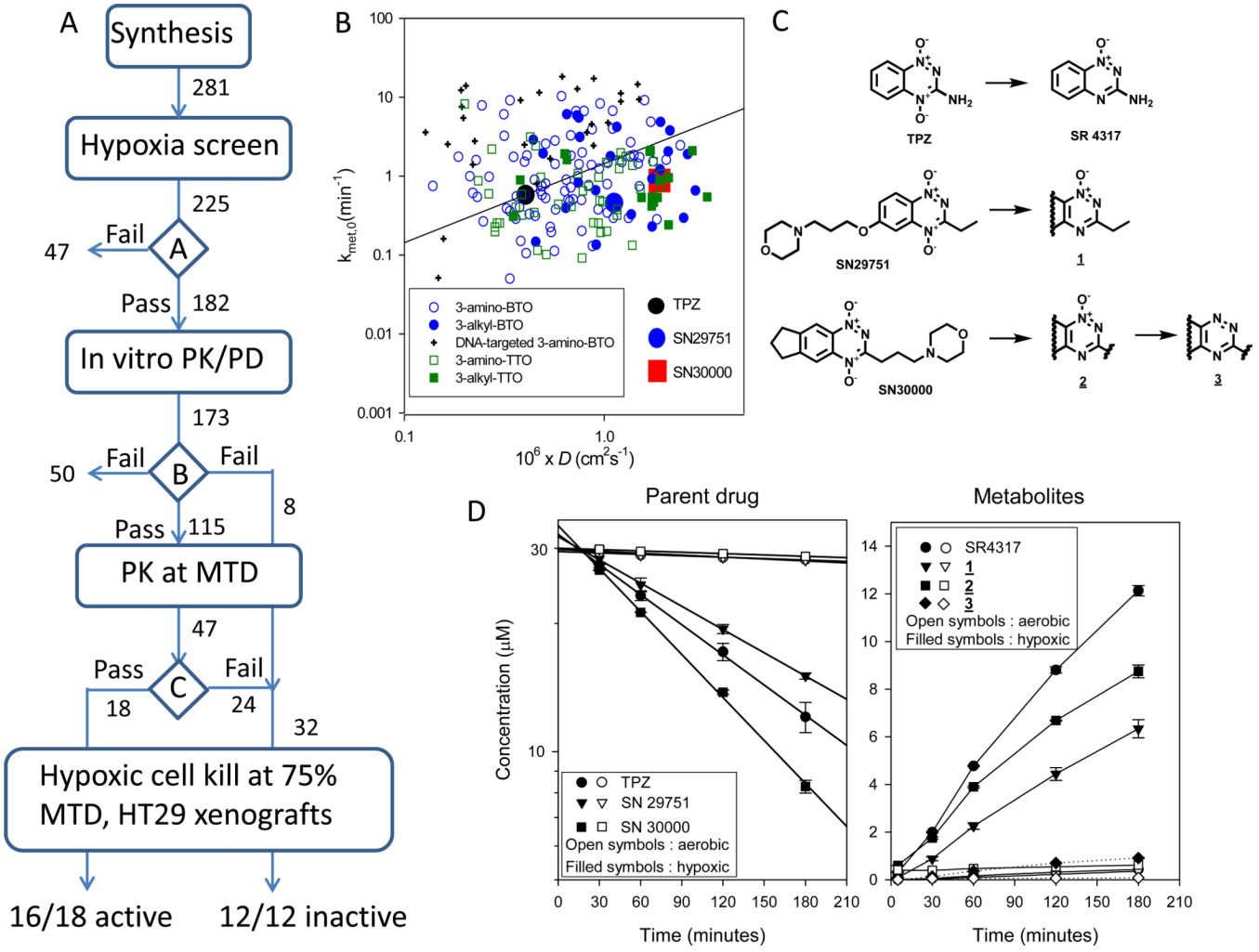

Figure 1.

Optimization of TPZ analogs and bioreductive metabolism of the identified lead candidates SN29751 and SN30000. A, SR-PKPD guided lead optimisation algorithm. See text for explanation. B, range of extravascular transport parameters (rate constant for reductive metabolism under anoxia $k_{met,0}$ and calculated tissue diffusion coefficient D) for compounds passing decision point 'A'. C, structures of TPZ, the lead 3-alkyl-BTO analog SN29751, the lead 3-alkyl-TTO SN30000, and their reduced metabolites. D, metabolism of TPZ, SN29751 and SN30000 in stirred suspensions of HT29 cells (2×10^6/ml) under aerobic and hypoxic conditions, determined by HPLC. Left panel: Parent di-N-oxides with regression lines to estimate k_{met}. Right panel: reduced metabolites. Values are mean and SEM for triplicate cultures.

A

Cell line	HT29 IC50 (μM)		SiHa IC50 (μM)	
	Aerobic	Hypoxic	Aerobic	Hypoxic
TPZ	352 ± 12	5.05 ± 0.17	203 ± 14	2.41 ± 0.18
SR4317	599 ± 37	>666	>666	>666
SN29751	781 ± 116	8.56 ± 1.11	626 ± 73	4.48 ± 0.42
1	417 ± 51	>550	>550	>550
SN30000	382 ± 54	3.75 ± 0.93	305 ± 21	1.51 ± 0.13
2	844 ± 60	924	986 ± 69	1020
3	714 ± 155	1300	667 ± 149	1190 ± 169

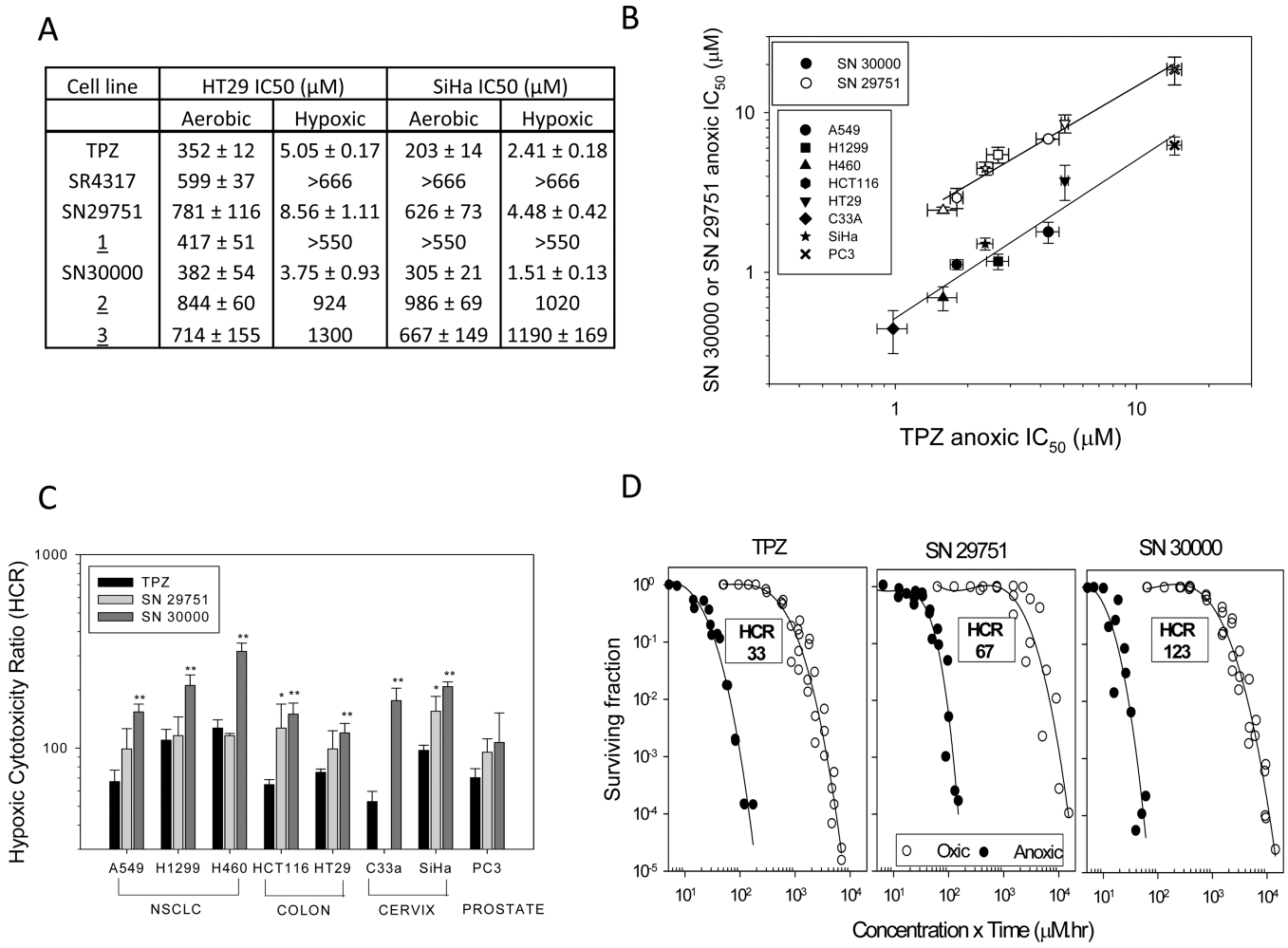

Figure 2.

Hypoxia-selective cytotoxicity of TPZ, SN29751 and SN30000 in human tumor cell cultures. Values are means and SEM for 2–10 experiments. A, IC_{50} for HT29 and SiHa cells following 4 h drug exposure under aerobic or hypoxic conditions. B, hypoxic IC_{50} in 8 human tumor cell lines. Lines are linear regressions. C, hypoxic cytotoxicity ratios (HCR, aerobic IC_{50}/hypoxic IC_{50}) in the same cell lines. Differences from TPZ by ANOVA: *, $p<0.05$; **, $p<0.01$. D, clonogenic survival of HT29 cells as a function of exposure under hypoxia (0% O_2) and oxic conditions (20% O_2).

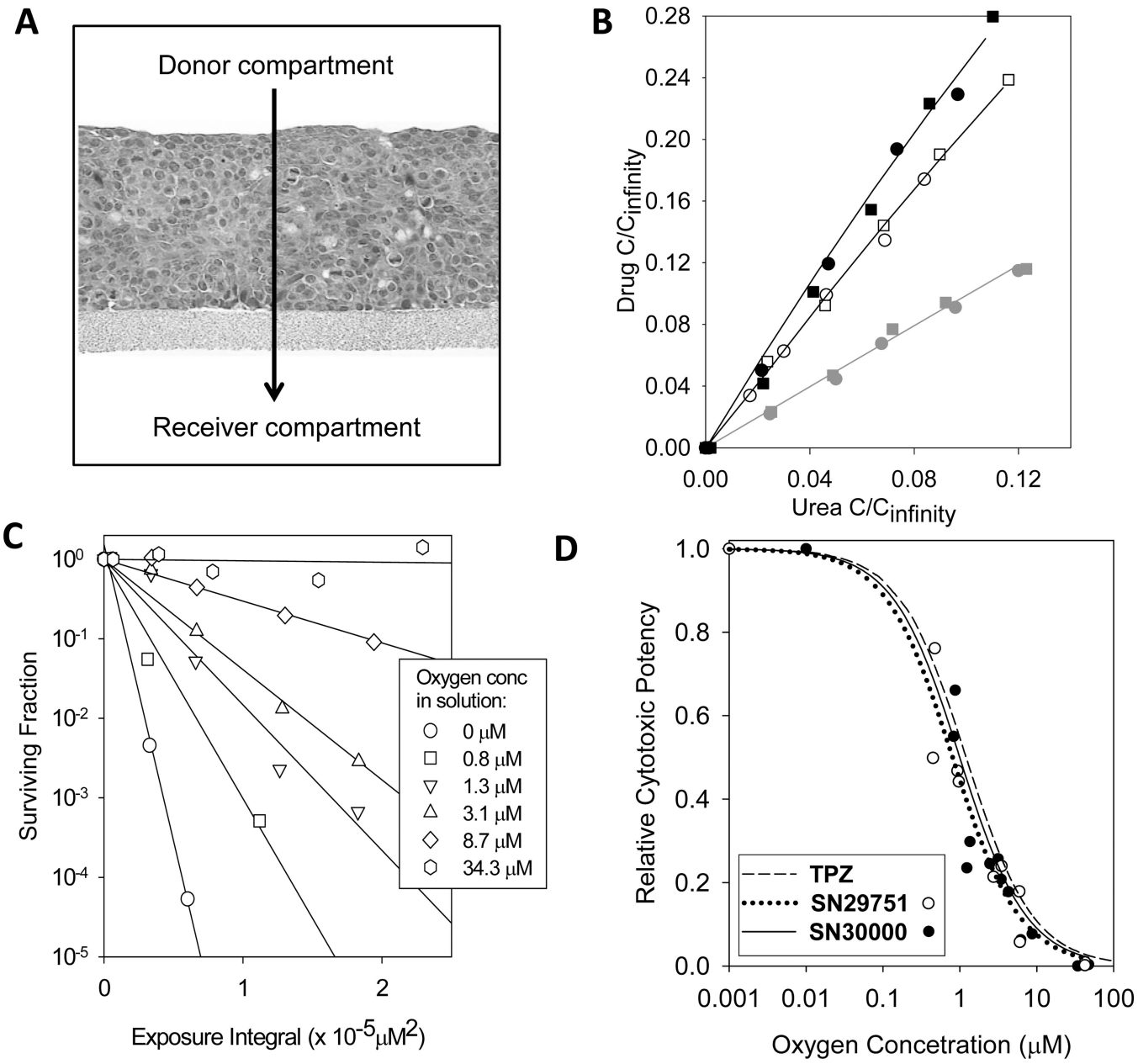

Figure 3.

Extravascular transport parameters for TPZ, SN29751 and SN30000. A, H&E stained section of an HT29 multicellular layer (MCL). The direction of drug transport in the diffusion chamber experiments is indicated by the arrow. B, concentration of TPZ (grey symbols), SN29751 (open symbols) and SN30000 (black, filled symbols) in the receiver compartment of diffusion chambers after flux through MCL. Concentrations are expressed as fractions of the expected concentration at equilibrium and plotted against the ^{14}C-urea internal standard (instead of time) to account for differences in MCL thickness. Two replicate experiments are shown (with different symbols) for each compound. C, surviving fraction data plotted against drug exposure integral (see Methods) for HT29 single cell suspensions exposed to SN30000 at the oxygen concentrations shown. D, oxygen dependence of cytotoxic potency for SN29751 (open symbols) and SN30000 (closed

symbols) compared with the previously reported values for TPZ determined using the same method (27). Curves are model fits with the K_{O2} as the fitted parameter.

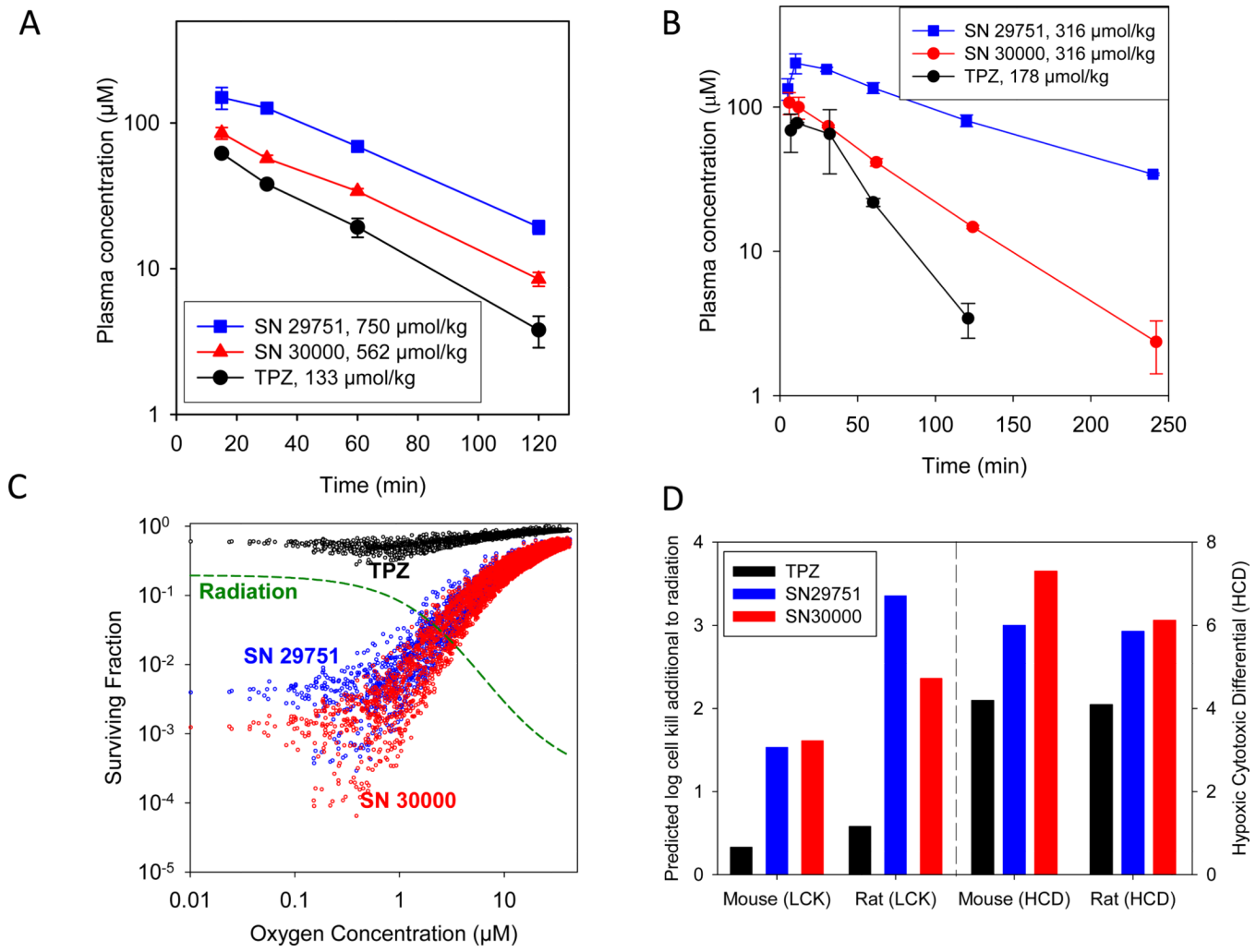

Figure 4.

Plasma PK of i.p. administered TPZ, SN29751 and SN30000 in mice and rats, and SR-PKPD model predictions. A, plasma PK at 75% MTD for male CD-1 nude mice (n=3 at each time). B, plasma PK at MTD for male Sprague-Dawley rats (n=2). C, predictions of the SR-PKPD model for cell killing in HT29 tumors (plotted as a function of oxygen concentration at each of 4000 grid positions in the microvascular network), based on plasma PK input in mice from A. D, predicted whole tumor average log cell kill (LCK) by the drugs when combined with radiation (additional to radiation only) in HT29 tumors, based on simulations in C. Selectivity is indicated by the hypoxic cytotoxicity differential (HCD) as defined in the text. Analogous simulation for an HT29-like tumor in male rats is based on the plasma PK in B.

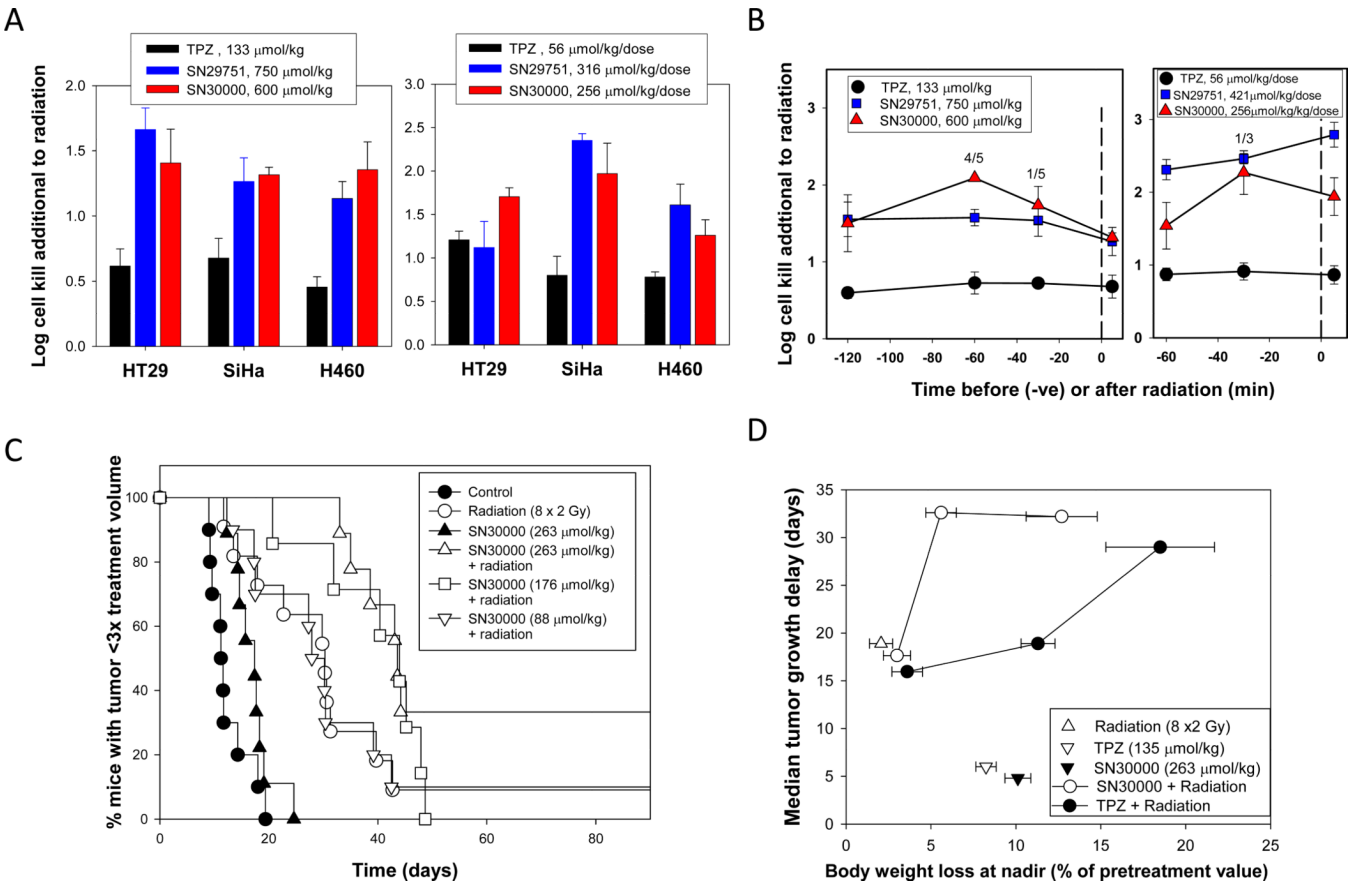

Figure 5.

Activity of TPZ, SN29751 and SN30000 against human tumor xenografts in combination with radiation. A, comparison of cell killing in three xenograft lines by tumor excision and clonogenic assay 18 h after the end of treatment (mean and SEM for 5 mice). Left: Single dose radiation (15 Gy for SiHa, 20 Gy for HT29 and H460), with compounds administered 5 min after irradiation. Right: Fractionated radiation (2.5 Gy×8), with compounds administered 30 min before each radiation dose. B, time course of interaction with radiation against SiHa tumors by excision assay (mean and SEM for 5 mice). Left: single radiation dose (15 Gy). Right: Fractionated radiation (2.5 Gy×8). Values above the points show the number of tumors excluded from analysis because <3 colonies were recovered. C, activity of SN30000 alone and 30 min before each dose of fractionated radiation (2 Gy × 8) against SiHa xenografts by tumor regrowth assay. Pooled data from two experiments, 7–11 mice/group. SN30000 alone at 263 μmol/kg/dose was not significantly active, but gave highly significant increases in radiation-induced tumor regrowth delay at both 263 and 176 μmol/kg/dose (p=0.0004 and 0.0058 respectively, log rank test). D, Comparison of regrowth delay of SiHa tumors and body weight loss at nadir. The SN30000 data are for the same experiments as C, which included TPZ groups at 45, 90 and 135 μmol/kg/dose using the same 8-dose schedule.

Table 1

Physicochemicalproperties of TPZ, SN29751 and SN30000, and SR-PKPD model parameters for prediction of hypoxic cell killing in HT29 xenografts in CD-1 male nude mice at 75% of MTD. Values are means and SEM (number of determinations in parentheses).

Parameter (units)	Description	TPZ	SN29751	SN30000
	Physicochemical properties			
MW (Da)	Molecular Weight	178	371	367
Solubility (mM)	Solubility in culture medium at 37°C	8.9 [a]	>46.7 [b]	48.5 [c]
E(1) (mV)	One electron reduction potential	−456 ± 8 [a]	−440 ± 9 [b]	−399 ± 8 [c]
Log P, pH 7.4	Octanol:water partition coefficient at pH 7.4	−0.34 ± 0.02 [a]	0.13 ± 0.01 [b]	0.50 ± 0.05 [c]
pKa	Calculated amine pK_a	NA	7.3	7.1[c]
HD, HA	Number of hydrogen bond donors, acceptors	2, 6	0, 8	0, 7
	SR-PKPD model parameters			
k_{met0} (min^{-1})	First order rate constant for prodrug metabolism under anoxia	1.30 ± 0.04 (74)	0.87 ± 0.03 (4)	1.53 ± 0.21 (8)
K_{O2} (μM)	O_2 concentration to halve anoxic cytotoxic potency	1.21 ± 0.09[d]	0.81 ± 0.19	1.14 ± 0.24
γ ($\times 10^{-5}$ μM^{-2})	Proportionality constant in PD model	2.41± 0.13 (72)	1.25 ± 0.31 (4)	5.34 ± 0.89 (13)
D ($\times 10^{-6}$ $cm^2 s^{-1}$)	Diffusion coefficient in HT29 MCLs and tumors	0.40 ± 0.02 (12)	1.07 ± 0.08 (4)	1.26 ± 0.11 (6)
ϕ	Cell volume fraction of HT29 MCLs and tumors	0.517[e]		
Dose (μmol/kg)	Dose corresponding to 75% of MTD, used for PK and PD evaluation in mice	133	750	562
C_{max} (μM)	Maximum plasma concentration in mice	61.7 ± 0.1	149.6 ± 25.6	85.1 ± 7.8
$AUC_{p\infty}$ (μM.h)	Area under the plasma (total drug) concentration-time curve extrapolated to infinity in mice	49	162	79
$t_{½}$ (min)	Plasma terminal half life in mice	27.9	34.8	32.1
θ %	Free fraction of drug in plasma in mice	100 ± 5.3 [f]	98 ± 2	83 ± 1

[a] From ref (39);

[b] From ref (40);

[c] From5;

[d] From ref (27);

[e] From ref (35);

[f] From ref (36)